

Image charge method based analytic model for imaging evaluation of pixellated CdZnTe detector

MIAO LI*, SHALI XIAO, XI WANG, LING NIE, YULIN CAO^a, YUXIAO CHEN^a, LIUQIANG ZHANG

Key Laboratory of Optoelectronic Technology and System, Ministry of Education, Chongqing University, Chongqing, China

^aInstitute of Electronic Engineering, China Academy of Engineering Physics, Mianyang, China

A novel analytic model which mainly considers the trapped carrier effect for the pixellated CdZnTe detector is obtained. The simulation results indicate that the rise of the photon energy reduces the signal modulation transfer function of the CdZnTe crystal (MTF_{CZT}). Obvious decline of the MTF_{CZT} was also found only when the electron mobility-lifetime product ($\mu_e\tau_e$) decreases to the order $10^{-5} \text{ cm}^2/\text{V}$ - $10^{-6} \text{ cm}^2/\text{V}$. The detailed analysis reveals that the deteriorations of the MTF_{CZT} , which resulted from the increase of the photon energy and the decline of the $\mu\tau$, mainly attribute to the decrease of the interaction probability and the aggravation of the carrier trapping effect. Moreover, a $40 \times 40 \text{ mm}^2$ CdZnTe imaging system has been established. The comparison of the presampling MTF shows that the simulation result is well consistent with the experimental data.

(Received March 29, 2011; accepted June 9, 2011)

Keywords: CdZnTe, Image charge method, Irradiation detector, Induced charge

1. Introduction

Pixellated CdZnTe detector is one of the most promising semiconductor devices for room temperature x- and γ -ray imaging detection [1]. In general application, a significant improvement has been achieved in CdZnTe crystal growth techniques over the past decade [2, 3]. However, there still lacks an intrinsic understanding about charge transport properties and the induced charge distribution under different conditions, let alone their influence on the detector imaging performance [4-6]. With an aim to evaluate the imaging detector performance, the charge carrier distribution is often obtained through the simulation to help analyse the induced signal distribution. With diffusion only, the x ray photon transport and the charge carrier transport in CdZnTe detector were modeled through the solution of the Poisson's equation and Monte-Carlo N-Particle (MCNPX) code in Alsager's work [7]. M. Beniut and L. A. Hamel presented a Monte Carlo algorithm based on Geant4 for the simulation of the charge collection behavior of the CdZnTe gamma detector [8]. However, these Monte-Carlo simulations are time-consuming and most of these models generate large amounts of data that must be properly analyzed for the evaluation of the detector performance. Thus, there is a pressing demand for a more flexible method of the CdZnTe imaging performance evaluation.

In this paper, a novel induced signal model for

pixellated CdZnTe imaging detector is presented. Based on the method of image charges, the analytic expression of presampling modulation transfer function (presampling MTF) for the detector is obtained. The influences of the trapped carriers on the imaging performance of the CdZnTe detector are investigated in detail. And the comparison between the simulation result and the experimental data is presented, indicating that the agreement is good.

2. Modeling

We considered the geometry of the induced charge model for the pixellated CdZnTe detector as shown in Fig. 1. The normalized coordinate in the Z direction was applied, and the origin position is the center of the cathode surface while there is a gap of negligible size between pixel anodes. When incident photon interacts with the CdZnTe crystal, the signal from the pixel electrode builds up while the electron and the hole drift towards anode and cathode separately. Each kind of free carriers contributes to the induced charge until the carriers are trapped or reach the electrode. The trapped carriers which are caused by poor transport properties induce signal in the near-the-incident-center area. This leads to the lateral signal spread, which results in the detector performance deterioration.

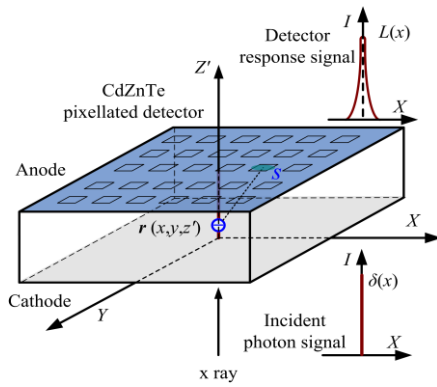


Fig. 1. Induced signal model of the CdZnTe pixellated detector.

By applying Green's theorem over the detector volume V , the signal charge on the element surface S can be expressed as [9]

$$Q_i = \frac{1}{4\pi} \int_S dS \left\{ \frac{\partial}{\partial z'_1} \left[\int_V G(r_1, r) \rho dV \right] \Big|_{z'_1=1} \right\} \quad (1)$$

This equation represents the induced charge signal caused by the trapped carrier with density ρ throughout the volume V . The Green function $G(r_1, r)$ represents the electrical potential at point $r_1(x_1, y_1, z'_1=1)$ on the anode surface. The potential is induced by the charge at point $r(x=0, y=0, 0 < z' < 1)$ in CdZnTe crystal as shown in Fig. 2.

For general application, we developed a more flexible method of potential calculation by firstly considering a point charge at random position $r_1(x_1, y_1, z'_1)$ in the detector bulk. As shown in Fig. 2, a convenient solution of the Green function could be obtained by constructing an infinite series of image charges, alternating from the positive to the negative, arrayed in the way that the potential adds up to zero on the anode surface ($z'_b=1$). Therefore, the Green function solution of random point $r_1(x_1, y_1, z'_1)$ in the CdZnTe detector is given by

$$G(r_1, r) = \sum_{k=-\infty}^{+\infty} \left[\frac{1}{\sqrt{(x_1-x)^2 + (y_1-y)^2 + [2k+(1-z'_1)+(1-z')]^2}} + \frac{1}{\sqrt{(x_1-x)^2 + (y_1-y)^2 + [2k-(1-z'_1)+(1-z')]^2}} \right] \quad (2)$$

It should be noted that the diffusion of carriers is negligible when compared with the drift of carriers under high voltage [10]. With drift only, all charge carriers would travel along a line which corresponds to the applied electric field. In the case that the trapped carriers are located in a line distribution with the density $\rho(z')$, the corresponding induced signal on the anode (where $z'_1=1$) has the general solution based on Eq.1 and Eq.2

$$Q_i = \frac{1}{2\pi} \int_0^1 -\rho(z') \sum_{k=-\infty}^{+\infty} \left\{ \frac{2k+(1-z')}{[x_1^2 + y_1^2 + (2k+1-z')^2]^{3/2}} \right\} dz' \quad (3)$$

And thus, considers the pitch space is negligible when compared with the pixel dimension, the X -axis direction line spread function (LSF) on the anode plane could be obtained by taking into account the induced charge effect which caused by the trapped carrier charges along the Z -axis.

$$L(x) = \frac{1}{2\pi} \int_{-\infty}^{+\infty} \int_0^1 -\rho(z') \times \sum_{k=-\infty}^{+\infty} \left\{ \frac{2k+(1-z')}{[x^2 + y^2 + (2k+1-z')^2]^{3/2}} \right\} dz' dy + Q_a \delta(x) \quad (4)$$

The second part Q_a refers to the equivalent charge signal resulted from untrapped charge carriers during the drift. Obviously, the trapped carriers density $\rho(z')$ and the Q_a should be obtained in normalized coordinate.

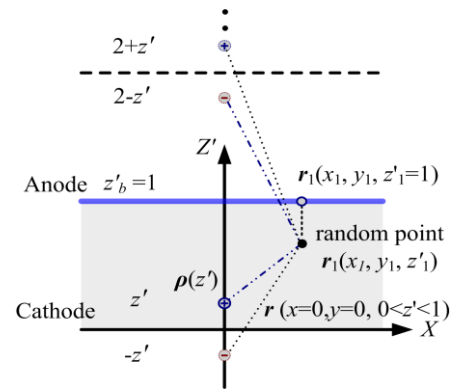


Fig. 2. Schematic of imaging charge method for the solution of Green function.

The concentrations of excess carriers in the CdZnTe detector were determined by solving the carrier continuity equations under the quasi-neutrality condition. The calculation assumed that the diffusion of carriers is negligible. The continuity equation for holes is given by [11]

$$\frac{\partial p(z, t)}{\partial t} = -\mu_h E \nabla p - \frac{p(z, t)}{\tau_h} \quad (5)$$

in which p is the density of holes, μ_h is the hole mobility, E is the applied field, and τ_h is the hole lifetime. Based on the boundary condition

$$p(z, 0) = N \exp(-\mu_a z) \quad (6)$$

the solution of Eq.5 for the drifting hole concentration is

$$p(z, t) = N \exp(-t/\tau_h) \exp[-\mu_a(z - \mu_h E t)] \quad \mu_h E t < z < L \quad (7)$$

in which N is the initial carrier concentration at $z=0$, and μ_a is the linear attenuation coefficient related to the incident photon energy. Thus, the trapped hole concentration at location z from the cathode surface is equal to

$$p_t(z) = \int_0^z \frac{\mu_h E}{\tau_h} N \exp[-\mu_a(z - \mu_h E t)] \exp(-t/\tau_h) dt \quad (8)$$

$$= N \frac{\exp(-\mu_a z) - \exp(-\frac{z}{\mu_h \tau_h E})}{1 - \mu_h \tau_h E \mu_a} \quad (9)$$

Since the calculation of the induced charge on the anode becomes too complicated when the initial carrier concentration N is incorporated. For simplicity, we normalized the initial carrier concentration N with the total initial carrier concentration which was uniformly distributed in the CdZnTe bulk. Thus the normalized trapping hole concentration could be written as

$$p'_t(z') = \frac{p_t(z')}{N'_0} = \frac{\exp(-z'/\alpha) - \exp(-z'/\lambda_h)}{\alpha[1 - \exp(-1/\alpha)](1 - \lambda_h/\alpha)} \quad (9)$$

$$N'_0 = \int_0^L N \exp(-\mu_a z) / L dz$$

in which $z'=z/L$, N'_0 is the total initial carrier concentration which assumed uniformly distributed along the CdZnTe bulk. L is the CdZnTe crystal thickness. $\alpha = 1/\mu_a L$ is the normalized absorption depth and $\lambda_h = \mu_h \tau_h E / L$ is the normalized mean free path of hole. Moreover, similar equations were solved for the normalized trapped electron concentration $n'_t(z')$ and the normalized equivalent signal charge of the untrapped electron concentration Q_a .

$$n'_t(z') = \frac{n_t(z')}{N'_0} = \frac{\exp(-z'/\alpha) - \exp[-(z'-1)/\lambda_e] \exp(-1/\alpha)}{\alpha[1 - \exp(-1/\alpha)](1 + \lambda_e/\alpha)} \quad (10)$$

$$Q_a = \int_0^1 \left[\frac{n(z'=0, t=0)}{N'_0} - n'_t(z') \right] dz' \quad (11)$$

$$= \frac{\lambda_e [1 - \exp(-1/\alpha - 1/\lambda_e)]}{\alpha [1 - \exp(-1/\alpha)] (1 + \lambda_e/\alpha)}$$

$\lambda_e = \mu_e \tau_e E / L$ is the normalized mean free path of electron.

By substituting Eq. 9-11 into Eq. 4, the detector LSF is determined. The induced signal modulation transfer function of the CdZnTe crystal (MTF_{CZT}) could be obtained by taking the modulus of the Fourier transform of the $LSF(x)$ and normalizing its value to 1 at zero spatial frequency. Thus, the Fourier transform of the $LSF(x)$ is

$$F(f) = \int_0^1 [-n'_t(z') - p'_t(z')] \frac{\sinh(2\pi f z')}{\sinh(2\pi f)} dz' + Q_a \quad (12)$$

in which f is the normalized spatial frequency. It should be noted that the formula

$$\operatorname{csch}(x) = 2 \sum_{k=0}^{+\infty} e^{(-2k+1)x}, x > 0 \quad (13)$$

was applied from integral tables [12] to simplify the expression of Eq. 12.

Consequently, the MTF_{CZT} is

$$MTF_{CZT}(f) = \frac{F(f)}{F(0)} \quad (14)$$

$$F(f) = \frac{\lambda_e [1 - e^{(-1/\alpha - 1/\lambda_e)}]}{(1 - e^{-1/\alpha})(\alpha + \lambda_e)} + \frac{1}{1 - e^{-1/\alpha}} \times$$

$$\left\{ \frac{e^{-1/\alpha} \alpha \left\{ -1 - 2\pi f \alpha [\cosh(2\pi f) - e^{1/\alpha}] \operatorname{csch}(2\pi f) \right\}}{(\alpha + \lambda_e) [(2\pi f)^2 \alpha^2 - 1]} + \right.$$

$$e^{-1/\alpha - 1/\lambda_e} \left\{ \frac{-2\pi f \lambda_e \operatorname{csch}(2\pi f)}{(\alpha + \lambda_e) [(2\pi f)^2 \lambda_e^2 - 1]} - \right.$$

$$\left. \frac{e^{1/\lambda_e} [1 - 2\pi f \lambda_e \coth(2\pi f)]}{(\alpha + \lambda_e) [(2\pi f)^2 \lambda_e^2 - 1]} \right\} +$$

$$\frac{e^{-1/\alpha} \alpha \left\{ 1 + 2\pi f \alpha [\cosh(2\pi f) - e^{1/\alpha}] \operatorname{csch}(2\pi f) \right\}}{(\alpha - \lambda_h) [(2\pi f)^2 \alpha^2 - 1]} +$$

$$\left. \frac{e^{-1/\lambda_h} \lambda_h \left\{ 1 + 2\pi f \lambda_h \operatorname{csch}(2\pi f) [\cosh(2\pi f) - e^{1/\lambda_h}] \right\}}{(-\alpha + \lambda_h) [(2\pi f)^2 \lambda_h^2 - 1]} \right\}$$

$$F(0) = \frac{1}{1 - e^{-1/\alpha}} \left\{ \frac{e^{-1/\alpha} \alpha (-1 - \alpha + \alpha e^{1/\alpha})}{-(\alpha + \lambda_e)} + \right.$$

$$\frac{e^{(-1/\alpha - 1/\lambda_e)} \lambda_e [-e^{1/\lambda_e} + (e^{1/\lambda_e} - 1) \lambda_e]}{-(\alpha + \lambda_e)} +$$

$$\left. \frac{e^{-1/\alpha} \alpha [1 + \alpha - \alpha e^{1/\alpha}]}{(\lambda_h - \alpha)} + \frac{e^{-1/\lambda_h} \lambda_h [1 + (1 - e^{1/\lambda_h}) \lambda_h]}{(\alpha - \lambda_h)} \right\}$$

$$+ \frac{\lambda_e [1 - e^{(-1/\alpha - 1/\lambda_e)}]}{(1 - e^{-1/\alpha})(\alpha + \lambda_e)}$$

Moreover, the presampling MTF of total imaging system, which considering the resolution limitation of the pixels, could be obtained by multiplying the MTF_{CZT} and the aperture MTF

$$MTF_{\text{presampling}}(f) = MTF_{CZT}(f) \times \left| \frac{\sin(\pi b f)}{\pi b f} \right| \quad (15)$$

in which b is the pixel size of detector.

3. Experimental

In order to evaluate the reliability of our model, the MTF data of practical CdZnTe pixellated detector was obtained according to our experimental system as shown in Fig. 3. The x ray source is the Eclipse IV (Rh target tube) from the Oxford Instruments. The anode voltage, the current and the exposure time were 45 kV, 40 μ A and 15 minutes, respectively. The pixellated CdZnTe detector (of 0.5 cm thickness) is provided by the Orbotech, and the pixel size is $0.93 \times 0.93 \text{ mm}^2$. With the application of a 1.5 mm-width slit collimator close to the cathode surface, the measured LSF data used to calculate the experimental

presampling MTF was acquired. To reduce the spatial noise influence, the LSF was sampled by averaging several LSF profiles. And hence, the presampling MTF of the imaging system could be obtained through the Fourier transform of the measured LSF data.

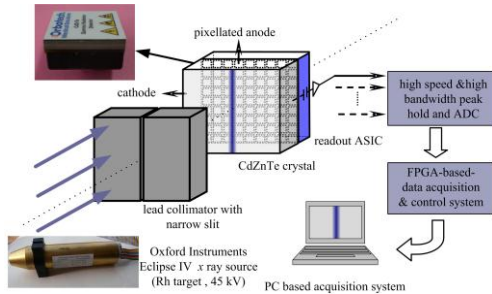


Fig. 3. Experimental set-up of the CdZnTe imaging system.

4. Results and discussion

Based on Eq.14, The MTF of the CdZnTe crystal response signal (MTF_{CZT}) was simulated firstly with different incident photon energies as shown in Fig. 4. The photon energy was varied from 10 keV to 200 keV. The mobility-lifetime products of electrons and holes were $\mu_e\tau_e = 5.0 \times 10^{-3} \text{ cm}^2/\text{V}$ and $\mu_h\tau_h = 2.0 \times 10^{-5} \text{ cm}^2/\text{V}$ respectively. The electric field we applied was the same as our experimental parameter, 2000 V/cm. Fig. 4 clearly illustrates that the MTF_{CZT} is deteriorated with the increase of photon energy and obviously suffers a steep fall from 60 keV to 125 keV. The reduction of the MTF_{CZT} may be ascribed to the discrepancy of the interaction probability. Because that the interaction probability of the low energy photon is higher than that of high energy photon in the CdZnTe crystal. The probability for 10 keV - 60 keV photons is in the range of 90%. This leads to a complete charge collection, and hence, a higher MTF_{CZT} . However, with a consecutive increase of the incident photon energy, the interaction probability rapidly decreases to 21.47 % for 200 keV photons, which leads to the deterioration of the MTF_{CZT} as shown in Fig. 4.

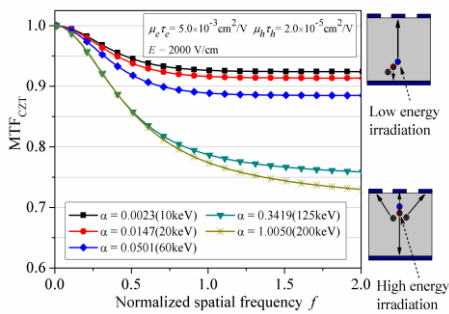


Fig. 4. MTF of the CdZnTe crystal for different incident photon energies.

Another important reason for the MTF_{CZT} deterioration is the increase of the trapped hole carriers

which results in the lateral spread of the induced signal. When the irradiated photon is 10 keV, most of the interactions occur near the cathode side. Excessive carriers are generated near the cathode surface and then traverse the CdZnTe crystal. During the carrier drift, the trapping effect of electrons is low because of the high mean free path and the influence of hole trapping is negligible because of the short drift length. Thus, the lateral spread induced signal resulted from trapping carriers is unobvious and the MTF_{CZT} is relatively high. In the case that the incident photon energy is higher, most of the interaction positions are relatively deeper. The drastic increase of trapped holes, which resulted from the relatively longer drift length, leads to a rise of the lateral spread induced signal at the anode plane. Consequently, the MTF_{CZT} declines with the increase of incident photon energy as shown in Fig. 4.

With the effect of the incident photon energy determined, we moved on to study the dependence of the MTF_{CZT} on the electron mobility-lifetime product ($\mu_e\tau_e$). As mentioned above, most of the interactions occur near the cathode side in the CdZnTe crystal when the irradiated photon energy is low. With the $\mu_e\tau_e$ of the order $10^{-3} - 10^{-4} \text{ cm}^2/\text{V}$ in practical CdZnTe crystal is determined, the electron transport in CdZnTe, in most cases, is unaffected by the carrier trapping. The mean free path of the electron is sufficiently high to transport electron carriers through the CdZnTe crystal for several mm or cm thick (λ_e and λ_h can be calculated from the $\mu\tau$ products by using the relation $\lambda = \mu\tau E$, where E is the electric field). And hence the decrease of $\mu_e\tau_e$ value in the range of 10^{-3} to $10^{-4} \text{ cm}^2/\text{V}$ has a very small effect on the induced signal of anode surface, let alone the MTF_{CZT} value. However, when the $\mu_e\tau_e$ decreases to the order $10^{-5} \text{ cm}^2/\text{V}$, which can be compared with the drift mobility-lifetime of hole ($\mu_h\tau_h$), the influence of excessive trapped electrons will be unnegligible.

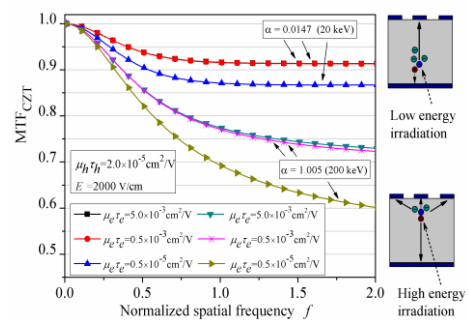
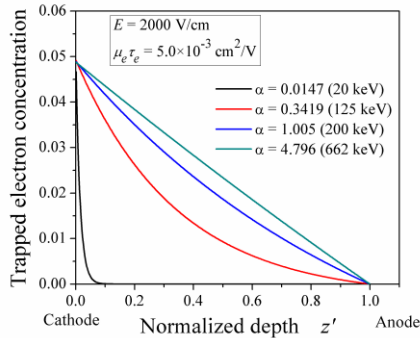


Fig. 5. MTF of the CdZnTe crystal with the decrease of $\mu_e\tau_e$ for different photon energies.

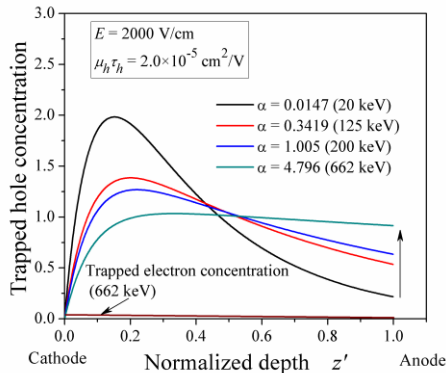
As other conditions under which the electric field is 2000V/cm and the $\mu_h\tau_h$ is $2.0 \times 10^{-5} \text{ cm}^2/\text{V}$, remained the same in Fig. 4, the MTF_{CZT} were simulated when the $\mu_e\tau_e$ altered from $5 \times 10^{-3} \text{ cm}^2/\text{V}$ to $0.5 \times 10^{-5} \text{ cm}^2/\text{V}$. Fig. 5 shows the comparison plot of the simulated MTF_{CZT} for different $\mu_e\tau_e$ values. It can be seen that the induced signal MTF of

the CdZnTe crystal, MTF_{CZT} , changes little while the $\mu_e\tau_e$ value varies from $5 \times 10^{-3} \text{ cm}^2/\text{V}$ to $0.5 \times 10^{-3} \text{ cm}^2/\text{V}$. However, when the $\mu_e\tau_e$ decreases to the order $10^{-5} \text{ cm}^2/\text{V}$ - $10^{-6} \text{ cm}^2/\text{V}$, both 20 keV and 200 keV energy interactions start suffering a rapid reduction in the MTF_{CZT} as is analyzed above.

To have a clear picture of the charge trapping effect in the CdZnTe crystal, the trapped carrier concentrations were calculated based on Eq. 9 and Eq. 10. Fig. 6 (a) and (b) show the trapped electron and hole concentrations with increasing incident photon energy, respectively.



(a) The trapped electron concentrations for different photon energies, $\mu_e\tau_e = 5 \times 10^{-3} \text{ cm}^2/\text{V}$.



(b) The trapped electron concentrations for different photon energies, $\mu_h\tau_h = 2.0 \times 10^{-5} \text{ cm}^2/\text{V}$.

Fig. 6. The trapped carrier concentrations with the increase of photon energy.

Apparently, the trapped electron concentration deep in the CdZnTe crystal rises with the consecutive increase of the incident photon energy as shown in Fig. 6 (a). The trapped electron concentration declines along the depth of the CdZnTe crystal for a changeless photon energy condition. However, it should be noted that the trapped electron concentration is negligible when compared to the trapped hole concentration. The effect of the different photon energies on the trapped hole concentration is shown in Fig. 6 (b). It can be seen that, with the increase of the irradiated energy, the trapped hole concentration near the cathode side is lower, while it is higher at the anode side. Therefore, we can infer from Fig. 6 (a) and (b) that the MTF_{CZT} deterioration, which resulted from the rise

of the photon energy as shown in Fig. 4, mainly attributes to the aggravated trapping effect of the hole carrier deep in the CdZnTe crystal.

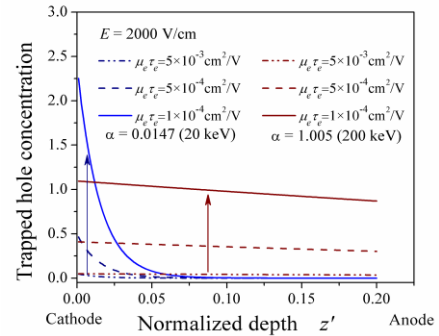
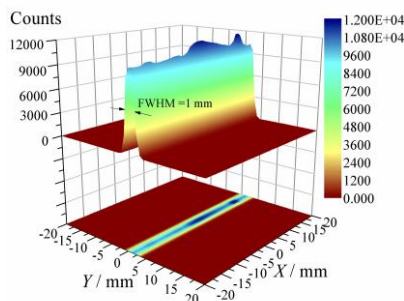


Fig. 7. Trapped electron concentrations with the decrease of the $\mu_e\tau_e$ for different photon energies.

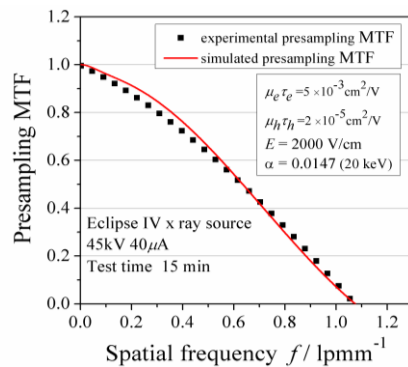
Fig. 7 clearly illustrates the trapped electron concentration under different $\mu_e\tau_e$ values for 20 keV and 200 keV photons. Obviously, the trapped electron concentration, which also indicates the probability of electron trapping, rapidly increases with the decline of the $\mu_e\tau_e$ under both low and high energy conditions. It's quite evident that, when the photon energy is 20 keV, the trapped electron decreases exponentially along the depth of the CdZnTe crystal. Though $\mu_e\tau_e$ reduces to $1.0 \times 10^{-4} \text{ cm}^2/\text{V}$, which results in a serious trapping effect, the distribution of trapped electron concentration is low and gradually negligible at the normalized depth $z = 0.075$. However, the trapped electron concentration is uniformly distributed along the crystal depth for 200 keV irradiated photons and the trapped electron exists for a longer range and in a much higher concentration. Thus, this leads to the aggravated trapping effect of drifting electrons deep in the CdZnTe bulk. Because the mean free path of the electron is shorter when the $\mu_e\tau_e$ is lower, more and more electrons are trapped during the carrier drift. The serious trapping effect of electron reduces the contrast of the detector output signal due to the incomplete charge collection, and also makes the spatial resolution in decline because of the intensified lateral spread of the induced signal as shown in Fig. 5.

Furthermore, the comparison between the simulated result and the experimental data was carried out for the reliability evaluation of our analytic model. According to the measurement system presented in Section 3, the LSF image of the slit imaging system is shown in Fig. 8 (a). The FWHM of the LSF is approximately 1 mm. Based on Eq.15, the simulation result of the system presampling MTF is also shown in Fig. 8 (b). The $\mu_e\tau_e$ and the $\mu_h\tau_h$, which applied in the simulation, were $5.0 \times 10^{-3} \text{ cm}^2/\text{V}$ and $2.0 \times 10^{-5} \text{ cm}^2/\text{V}$ respectively [13]. The CdZnTe crystal thickness L was 5 mm. And the applied high voltage, which chosen deliberately in calculation as same as the experimental parameter, was 1000 V. As can be seen, a reasonable agreement between the simulated result and the experimental data could be found in Fig. 8 (b). The

simulated presampling MTF is slightly higher than the experimental data in the range of spatial frequency $f < 0.6$ lpmm⁻¹. This is probably caused by the discrepancy of the photon energy between the practical value and the energy value used in simulation. It should be noted that the Rh-K α line and Rh-K β line, which are emitted from the polyenergetic x ray source under 45KV voltage, are 20.2 keV and 22.72 keV respectively. The linear attenuation coefficient of the CdZnTe crystal which applied in the simulation is 136 cm⁻¹ for 20 keV photon energy approximately. Just in line with the analysis about Fig. 4, the decline of the interaction probability which caused by the increase of photon energy leads to incomplete charge collection deep in the CdZnTe crystal, and hence, results in the deterioration of the imaging performance.



(a) Measured LSF image with the Orbotech pixellated detector



(b) The comparison of the total system presampling MTF

Fig. 8. Experimental data obtained by the Orbotech pixellated detector and the comparison result.

5. Conclusion

Based on the image charge method, a novel induced signal model which mainly takes into account the carrier trapping effect in the pixellated CdZnTe detector is presented. The MTF_{CZT} and the trapped carrier concentration are investigated in detail. The simulation results indicate that the MTF_{CZT} decreases with increasing incident photon energy due to the aggravated trapping effect of the hole carriers deep in the CdZnTe crystal and the decline of the photon interaction probability. It's also

been found that the reduction of the $\mu_e\tau_e$ which varies from 5×10^{-3} cm²/V to 0.5×10^{-3} cm²/V has small effect on the MTF_{CZT} . However, when the $\mu_e\tau_e$ decreases to the order 10^{-5} cm²/V- 10^{-6} cm²/V, excessive trapped electrons make the MTF_{CZT} in decline obviously due to the incomplete charge collection and the lateral spread induced signal on the anode plane. Moreover, the comparison between the simulated presampling MTF and the experimental data is accomplished. The result shows that the induced signal model is reliable. The optimization of our analytic model which considering the diffusion effect under low electric field condition is under studied and the further applications on the pixellated CdZnTe imaging detector are expected in the near future.

Acknowledgements

This work was supported by the National Natural Science Foundation & China Academy of Engineering Physics Foundation (the NSAF) under Grant No.10876044, the Fundamental Research Funds for the Central Universities of China under Grant No. CDJXS11122219.

References

- [1] S. D. Sordo, L. Abbene, E. Caroli, A. M. Mancini, A. Zappettini, P. Ubertini, *Sensors* **9**, 3491 (2009).
- [2] D. S. Bale, *J. Appl. Phys.* **107**, 014519 (2010).
- [3] Y. D. Xu, W. Q. Jie, P. J. Sellin, T. Wang, W. H. Liu, G. Q. Zha, P. Veeramani, C. Mills, *J. Phys. D Appl. Phys.* **42**, 035105 (2009).
- [4] J. Hong, B. Allen, J. Grindlay, N. Chammas, S. Barthelemy, R. Baker, N. Gehrels, K. E. Nelson, S. Labov, J. Collins, W. R. Cook, R. McLean, F. Harrison, *Nucl. Instr. and Meth. in Phys. Res. A* **605**, 364-373 (2009).
- [5] M. Prokesch, D. S. Bale, C. Szeles, *IEEE Trans. Nucl. Sci.* **57**, 2397 (2010).
- [6] M. Li, S. L. Xiao, L. Q. Zhang, Y. L. Cao, Y. X. Chen, M. Shen, X. Wang, *Chin. Phys. Lett.* **27**, 070702 (2010).
- [7] A. A. Alsager, N. M. Spyrou, *Nucl. Instr. and Meth. in Phys. Res. A* **580**, 462 (2007).
- [8] M. Benoit, L. A. Hamel, *Nucl. Instr. and Meth. in Phys. Res. A* **606**, 508 (2009).
- [9] J. D. Eskin, H. H. Barrett, H. B. Barber, *J. Appl. Phys.* **85**, 647 (1999).
- [10] S. M. Sze, Kwok K. Ng, *Physics of Semiconductor Devices*, John Wiley & Sons Press, New York (2007).
- [11] Y. Cui, M. Groza, D. Hillman, A. Burger. *J. Appl. Phys.* **92**, 2556 (2002).
- [12] I. S. Gradshteyn, I. M. Ryzhik. *Table of Integrals, Series, and Products*, Academic Press, New York (1980).
- [13] K. A. Jones, A. Datta, K. G. Lynn, L. A. Franks, *J. Appl. Phys.* **107**, 123714 (2010).

*Corresponding author: czt.cqu@gmail.com